Magnetic and electrical bistability in hybrid composites of conducting polymers with [Fe(NH$_2$–trz)$_3$]$_n$[SO$_4$]$_n$

David Nieto–Castro, *[a] Anna Graf, Francesc Gispert-Guirado[b] and José Ramón Galán–Mascarós *[a,c]

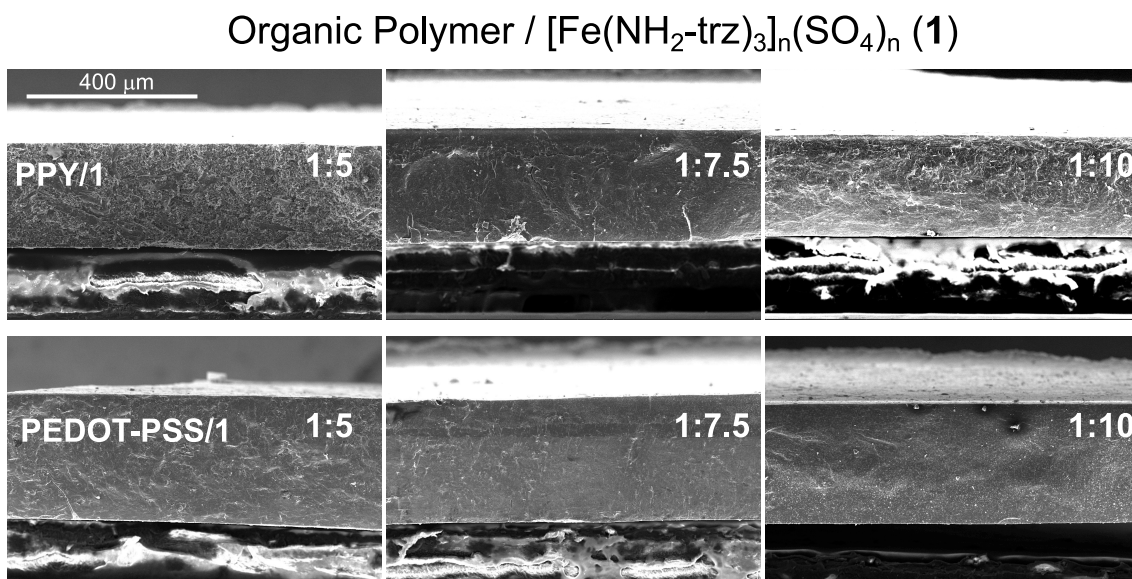## Organic Polymer / [Fe(NH$_2$-trz)$_3$]$_n$(SO$_4$)$_n$ (1)

Figure S1. ESEM cut section images of organic polymer/**1** composites.
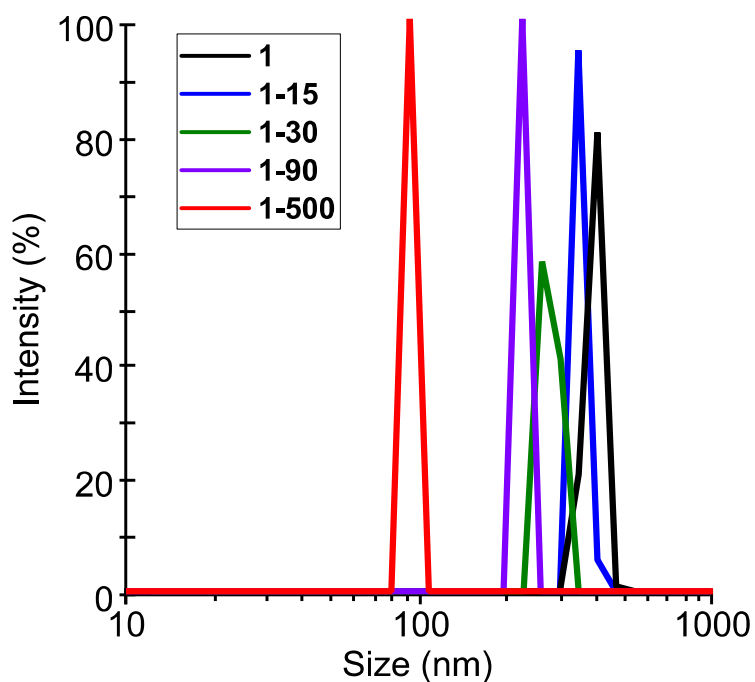

Figure S2. Particle size distribution for colloidal suspensions of **1**, **1-15**, **1-30**, **1-90** and **1-500** determined by DLS analysis

Table S1. Average particle size distribution for each sample as determined by DLS

Sample	Size (nm)
1	385.6
1-15	345.0
1-30	314.6
1-90	220.2
1-500	91.3

Crystal Structure of [Fe(NH₂trz–trz)₃]ₙ[SO₄]ₙ in HS

The crystal structure of $[Fe(NH_2-trz)_3]_n[SO_4]_n$ (**1**) in the LS state was reported with a *P6₃/m* space group with two formula units per cell. We were able to obtain the PXRD diffractogram of **1** at 400 K (HS state). The PXRD analysis was performed from 8 to 72° *2θ* with a step size of 0.03° with different acquisition times (for 8−70° at 12s, for 40−52° at 24s and for 52−72° at 30s) in order to enhance the peak/noise ratio. The three patterns were refined simultaneously, TOPAS 6.0 based on the Rietveld method,[1] with the *P6₃/m* space group. Figure S4.3 shows the coordination network where Fe(II) centers are connected by $4-NH_2-1,2,4-$triazole molecules, creating a polymer chain. The sulfate counteranions are disordered between two positions in the interspace among the polymer chains. The main differences with the structure in the LS state are a higher cell volume due to the population of the Fe(II) e_g orbitals that have an antibonding character and interact with nitrogen orbitals, and a bending in the angle of the $4-NH_2-1,2,4-$triazole amino radical.
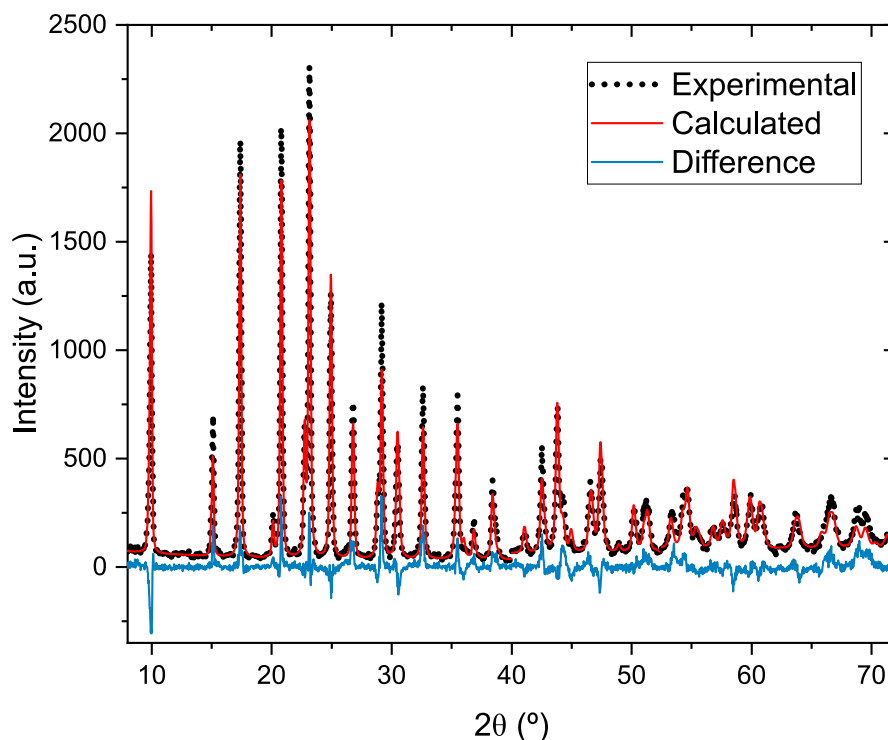
Figure S3. Experimental (black dots) and calculated (red line) diffraction patterns of **1** in the HS state. The difference pattern divided by signal to noise ratio is shown as a blue line.
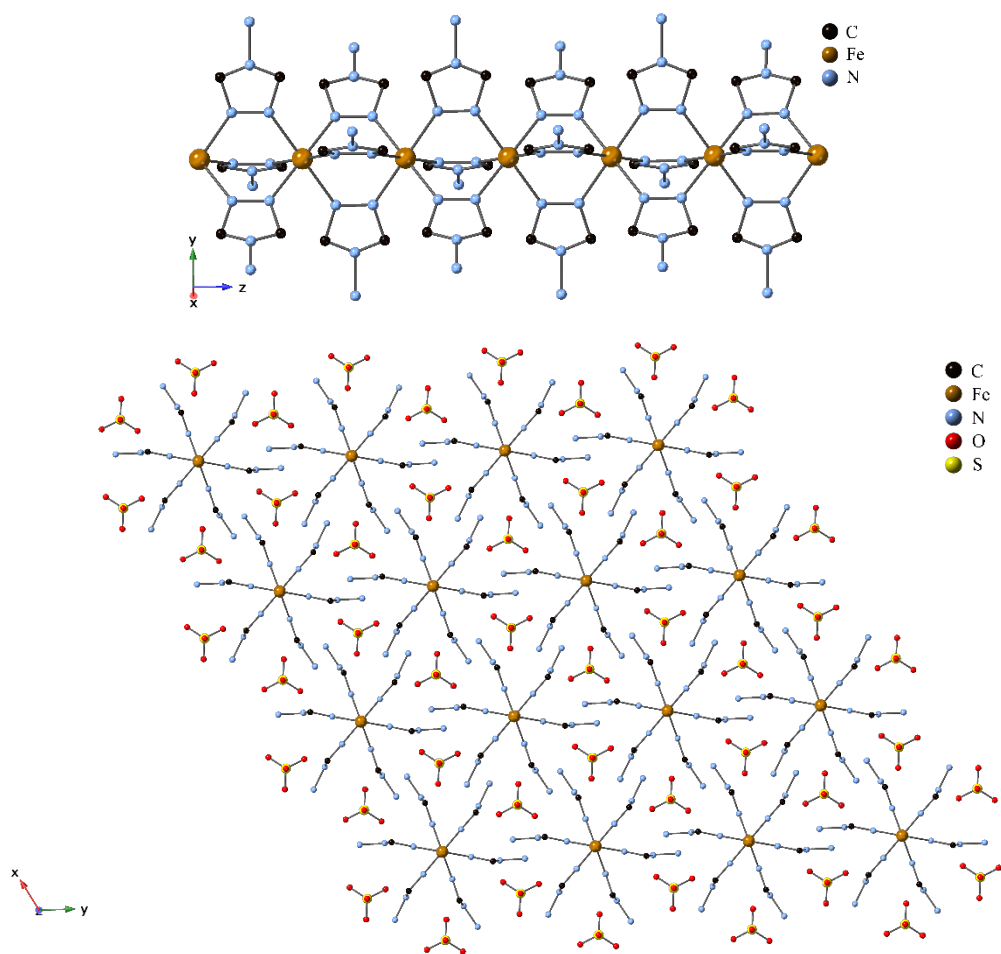
Figure S4. Crystal structure of $[Fe(NH_2-trz)_3]_n[SO_4]_n$ (**1**) in the HS state along the z axis (top) and crystal packing of the polymer chains along the y axis (bottom).

Table S2. Crystal unit cell and Rietveld refinement data obtained for **1** in HS.

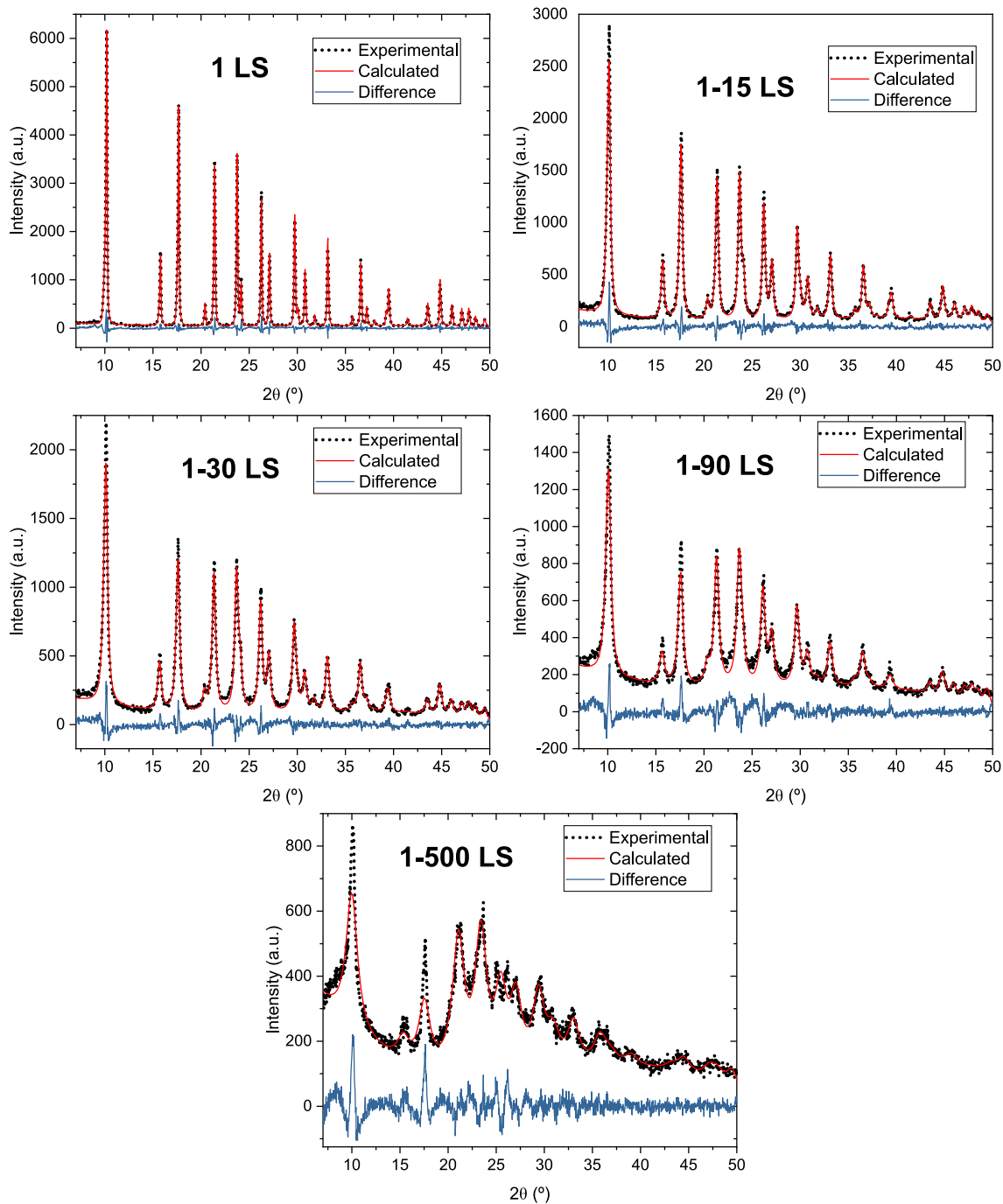| Temperature	400 K	Z	2
Crystal system	Hexagonal	2θ Angular range [°]	8–72
Space group	$P6_3/m$	R_{wp}	15.68
	$a = b = 10.1196(6)$	R_p	12.68
Cell parameters	$c = 7.7716(6)$	Volume [Å³]	689.23(10)
	$\alpha = \beta = 90°$		
	$\gamma = 120°$		

Figure S5. Pawley refinement plot of X-ray Diffraction data of **1** and its milled samples in LS.
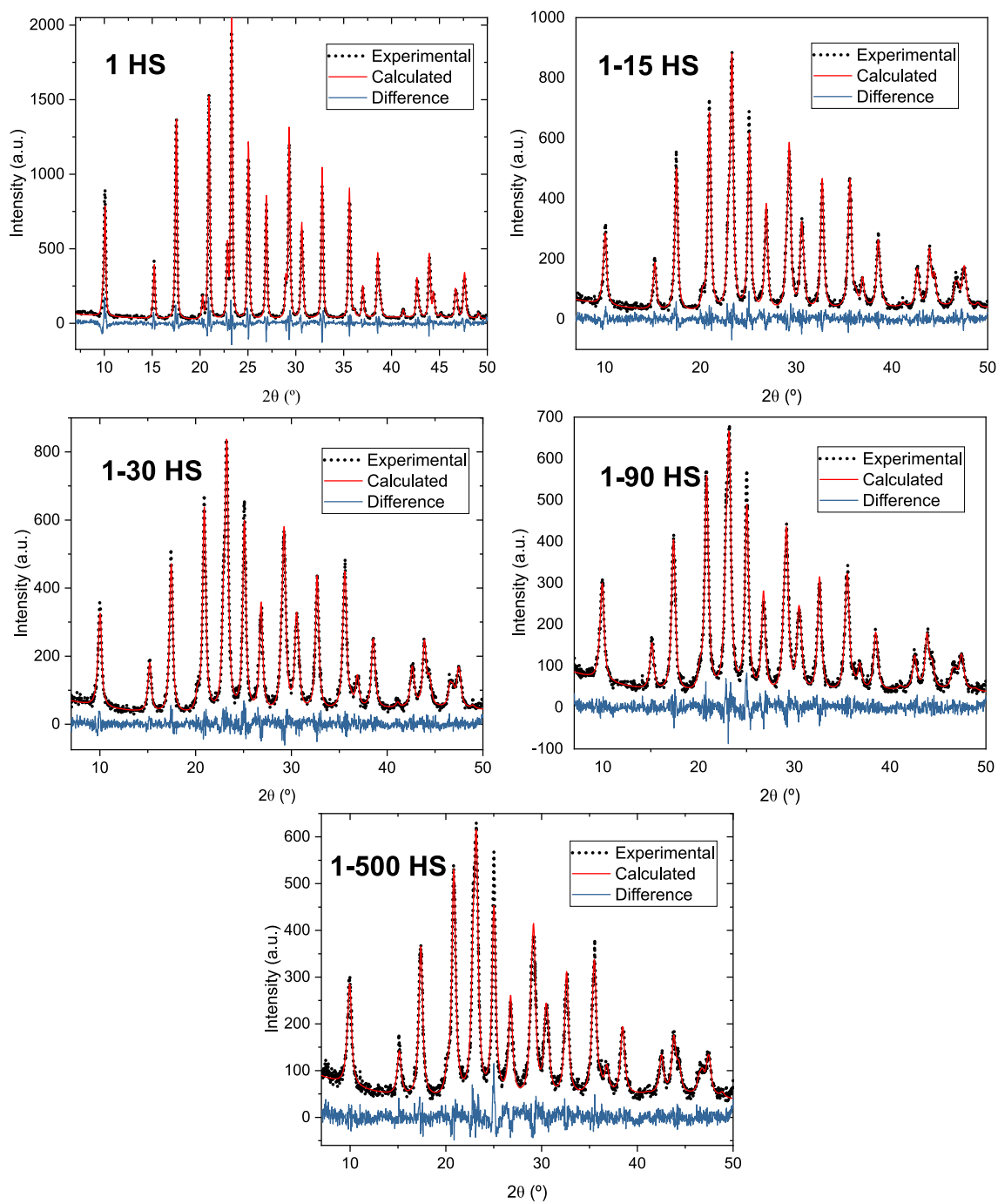
Figure S6. Pawley refinement plot of X-ray Diffraction data of **1** and its milled samples in HS.
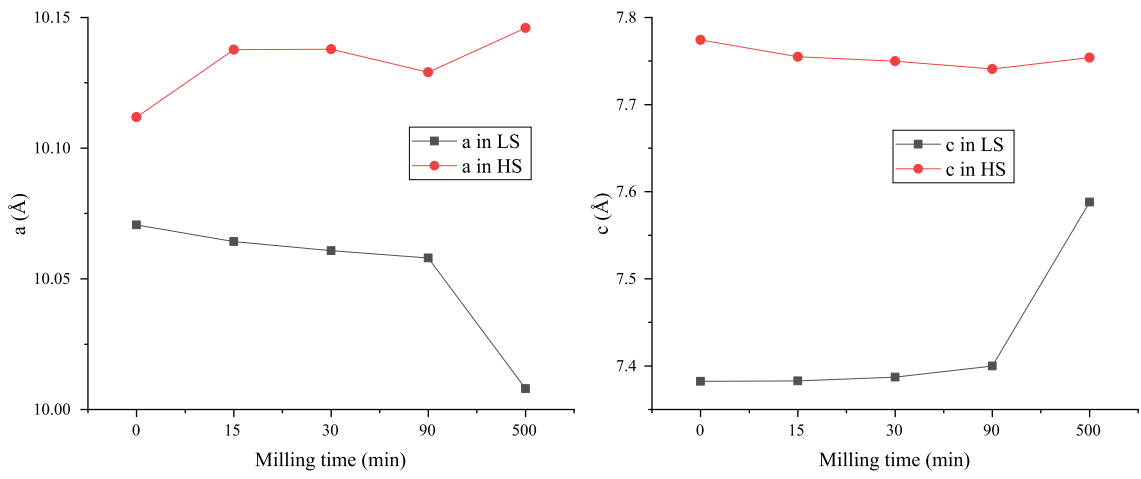
Figure S7. *a* and *c* evolution upon grinding obtained from Pawley refinement.

Temperature-independent residual paramagnetism corrections

The residual paramagnetic impurities in the SCO systems are very high, we experimentally subtracted the residual constant for every sample using the Curie-Weiss law:

$$\chi = \frac{C}{(T - \theta)} + \chi_{residual}$$
Equation S1

where *C* is the Curie constant, θ is the correction term or Weiss constant and $\chi_{residual}$ is the magnetic susceptibility of the residual temperature-independent paramagnetism. The residual corrections corrections were performed sustracting the intercept in the x axis of the plots to the original χ values.
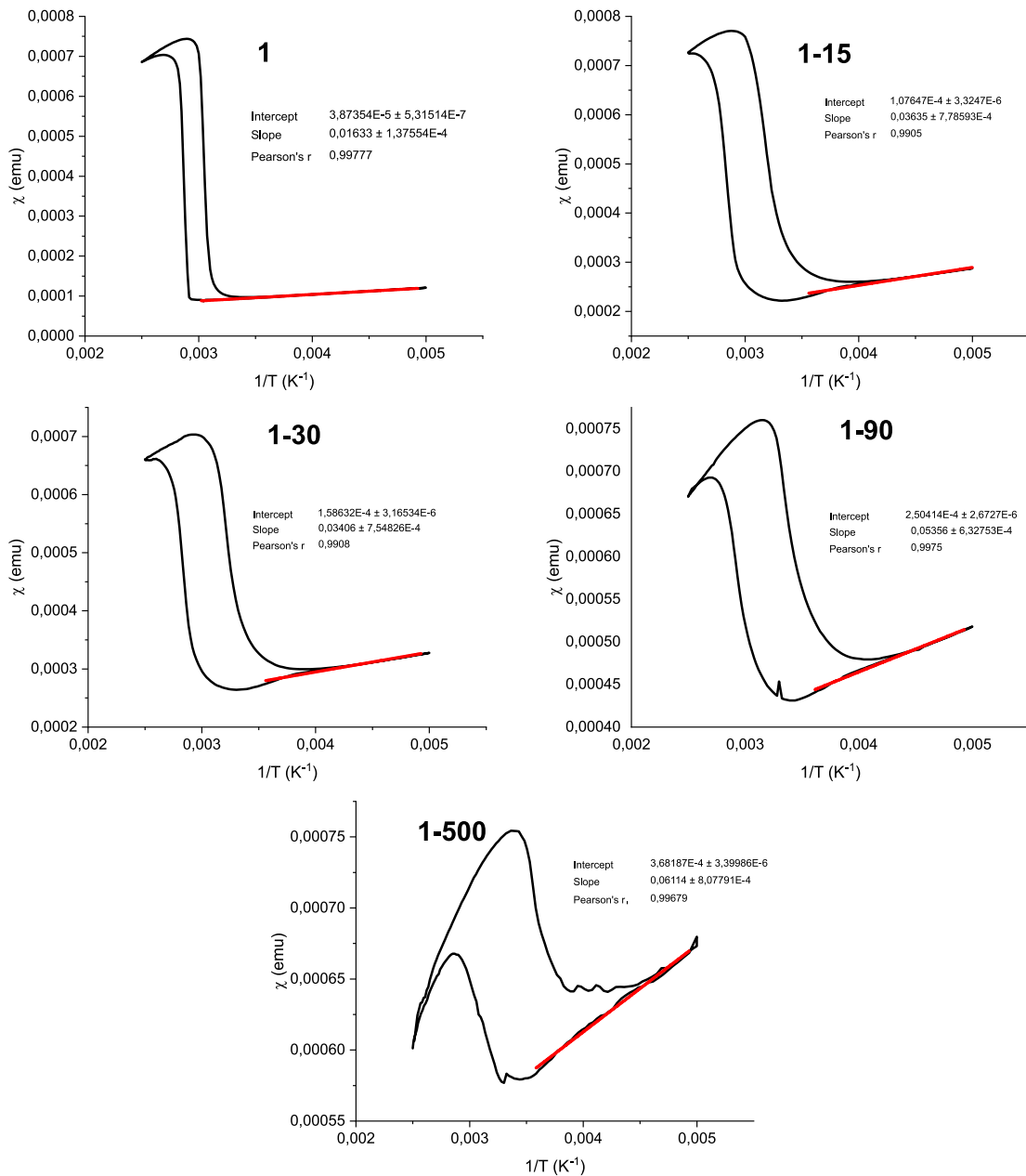

Figure S8. *χ* vs *1/T* of the last cycle and the residual temperature-independent paramagnetism correction (red line) of **1** and its milled samples.
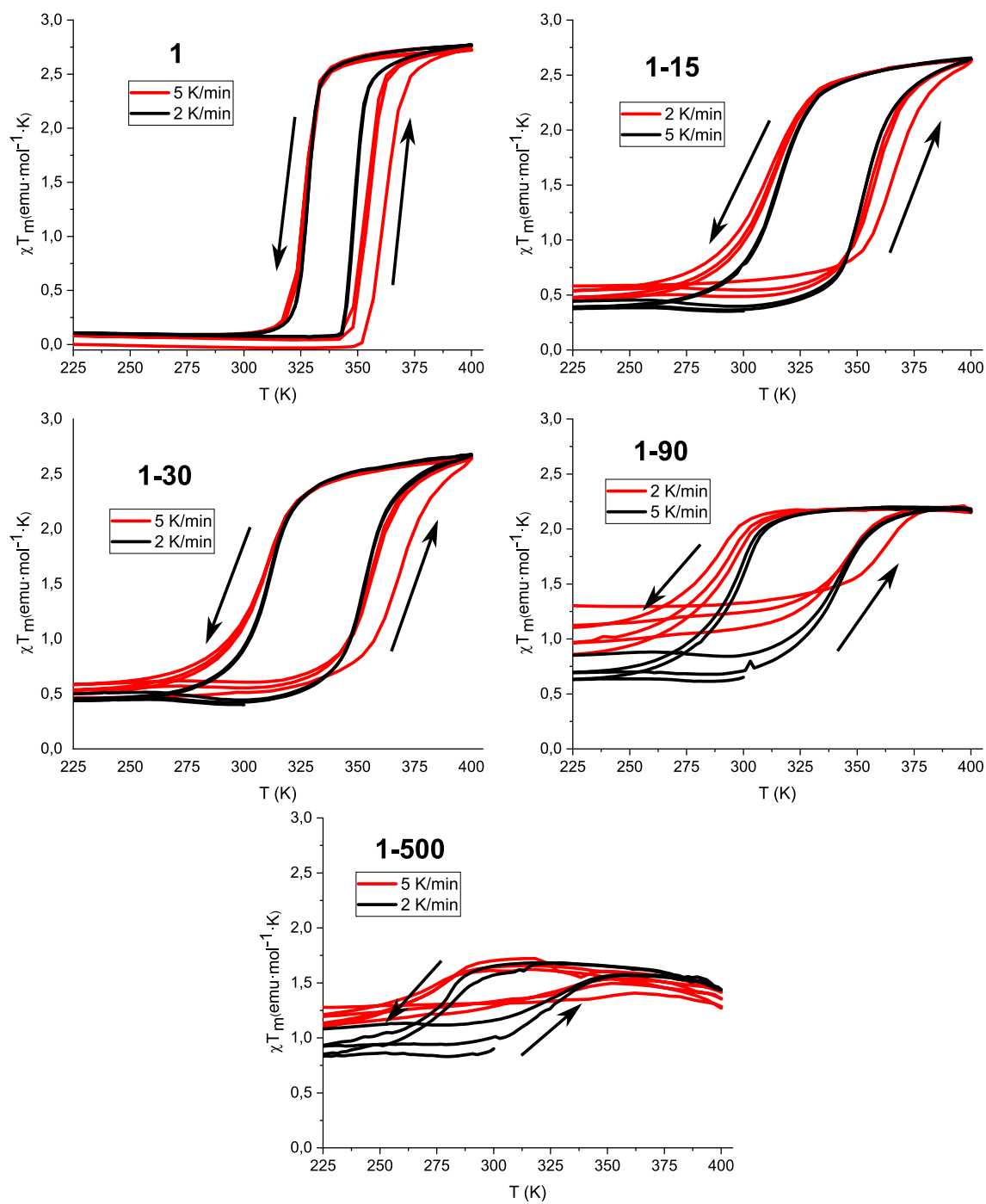
Figure S9. $\chi_m T$ vs T cycles of **1** and its milled samples in the 225–400 K region (first two cycles were performed at 5 K/min and the rest at 2 K/min).

Slichter and Drickamer model

This model is based on the assumption that HS and LS states are statistically distributed and form regular solutions. At equilibrium, this model leads to the equation S2:

$$ln\left(\frac{1-\gamma_{HS}}{\gamma_{HS}}\right) = \frac{\Delta H + \Gamma(1-2\gamma_{HS})}{RT} - \frac{\Delta S}{R}$$

Equation S2

Where:

$$\gamma_{HS} = \frac{\chi T - \chi T_{LS}}{\chi T_{HS} - \chi T_{LS}} \qquad \Delta H = \frac{|\Delta H\uparrow| + |\Delta H\downarrow|}{2} \qquad \Delta S = \frac{\Delta H}{T_c}; \; T_c = \frac{T_{1/2}\uparrow + T_{1/2}\downarrow}{2}$$

Γ, is the mean field interaction parameter that measures the cooperatitivy. If $\Gamma>2RT_c$, the transition occurs with hysteresis, when $\Gamma<2RT_c$, the transition is gradual and if $\Gamma=2RT_c$, the transition is abrupt without hysteresis.

Equation S2 was converted into equation S3 for an effective fitting.

$$T = \frac{\Delta H + (1-2\gamma_{HS})\Gamma}{S + Rln(\frac{1-\gamma_{HS}}{\gamma_{HS}})}$$

Equation S3

Γ was determined with equation S3 and with the experimental values of γ_{HS} vs T (figure S11 and S12).
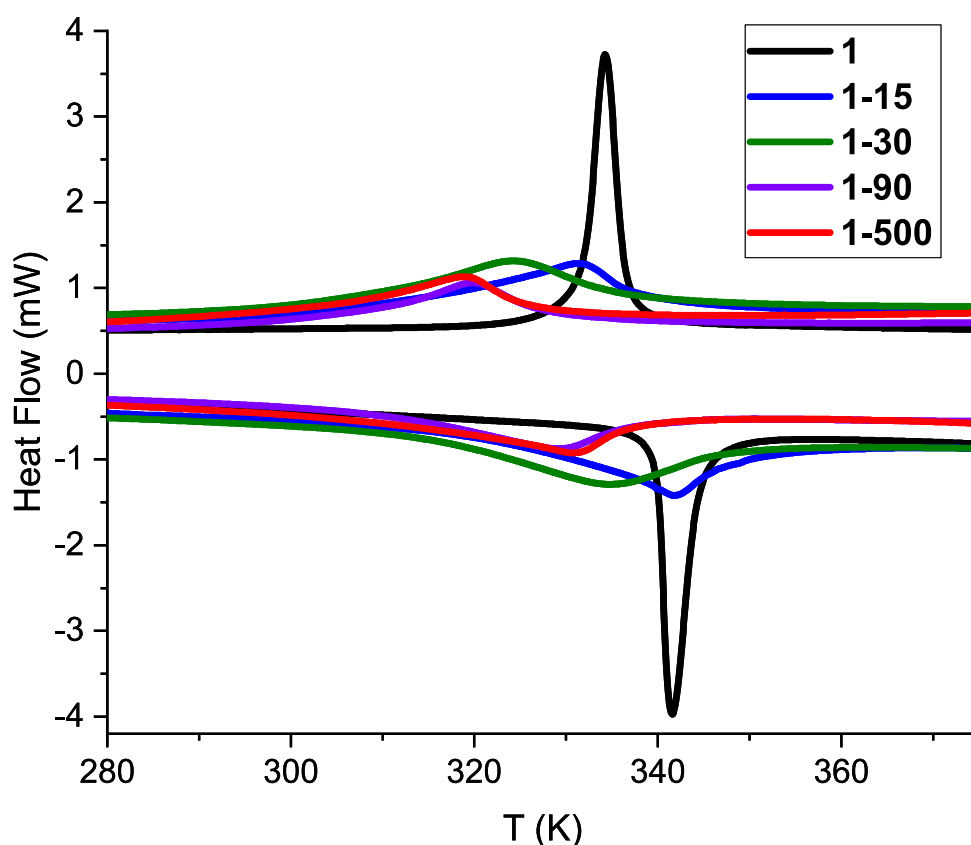

Figure S10. DSC cycles in the range from 280 to 375 K (Scan rate 2 K/min) for **1** and all the milled samples.
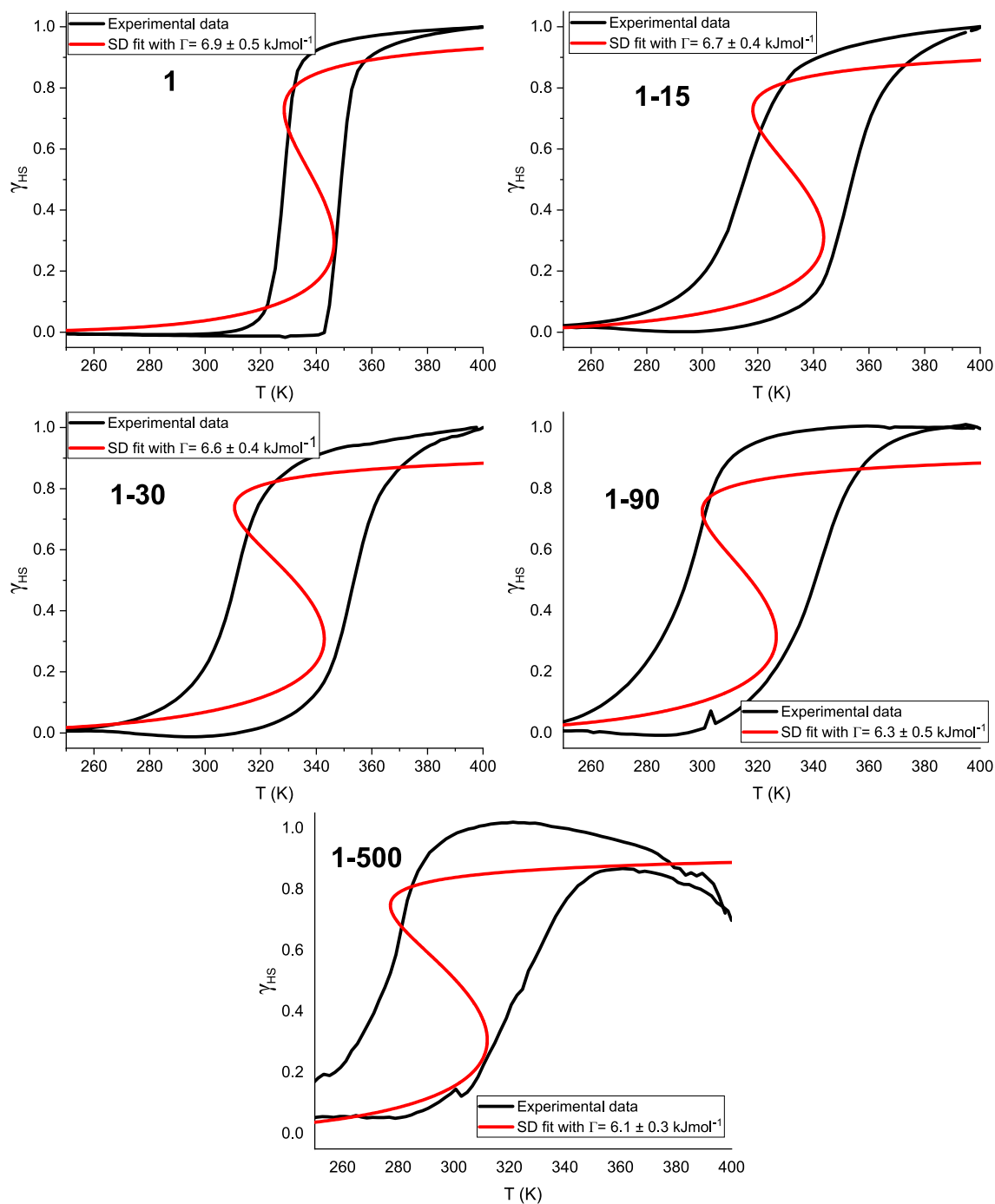
Figure S11. Slichter Drickamer fittings of **1** and its milled samples.

Table S3 parameters for the Slichter and Drickamer modelling of **1**.

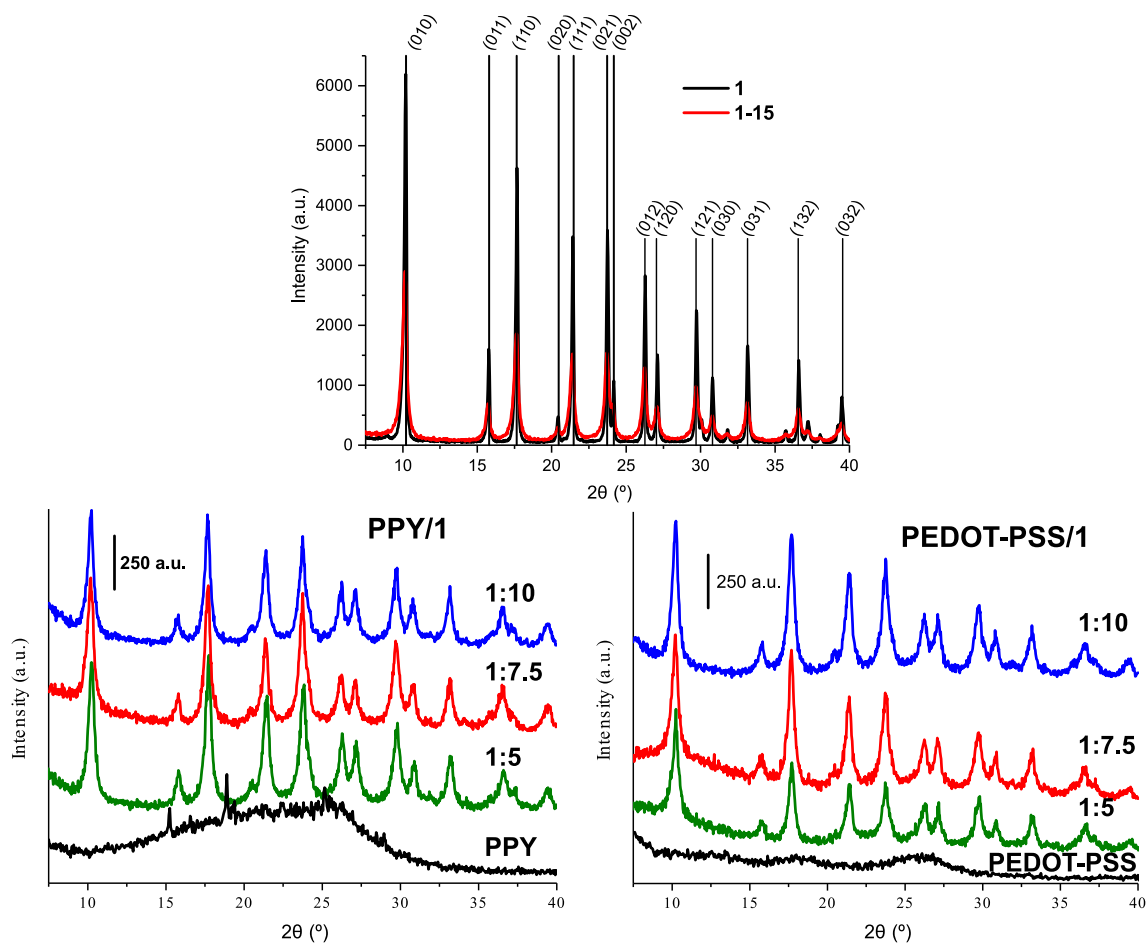| Sample	$T_{1/2}(\uparrow)$ [K]	$T_{1/2}(\downarrow)$ [K]	T_c [K]	ΔH[kJ mol^{-1}]	ΔS [kJ K^{-1} mol^{-1}]	Γ [kJ mol^{-1}]
1	349	329	339	14.70	0.044	6.9 ± 0.5
1-15	352	315	334.5	8.99	0.027	6.7 ± 0.4
1-30	352	310	331	7.84	0.024	6.6 ± 0.4
1-90	340	295	317.5	7.41	0.023	6.3 ± 0.5
1-500	326	279	301	6.56	0.022	6.1 ± 0.3

Figure S12. PXRD of **1**, **1-15**, the organic polymers and the organic polymer/**1** composites. (ratio Polymer:SCO)
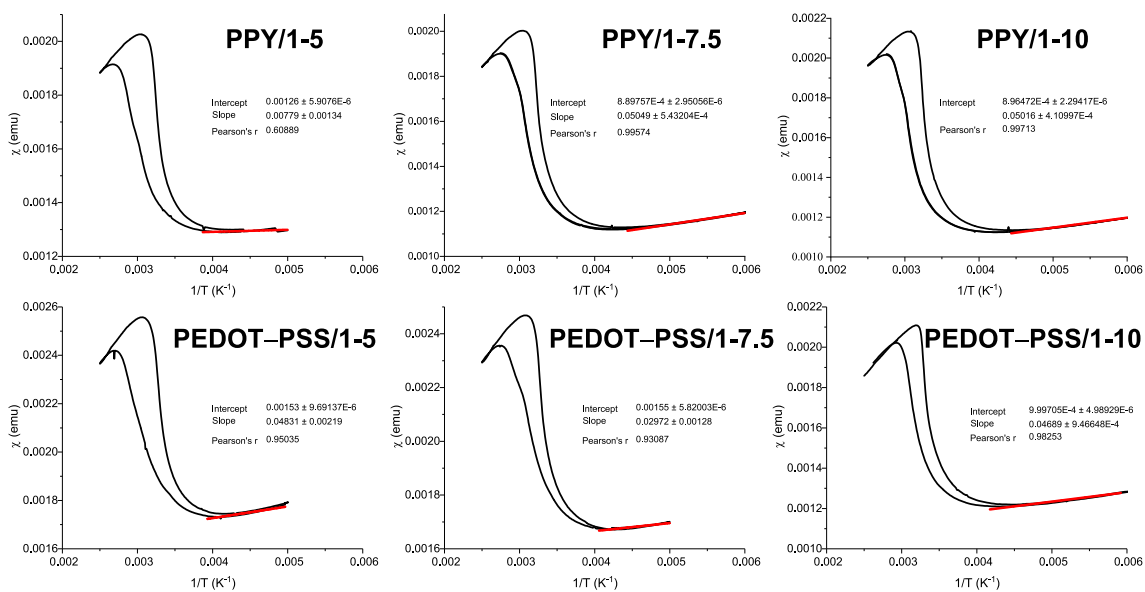

Figure S13. χ vs $1/T$ of the last cycle and the residual correction (red line) of the organic polymers/**1**.
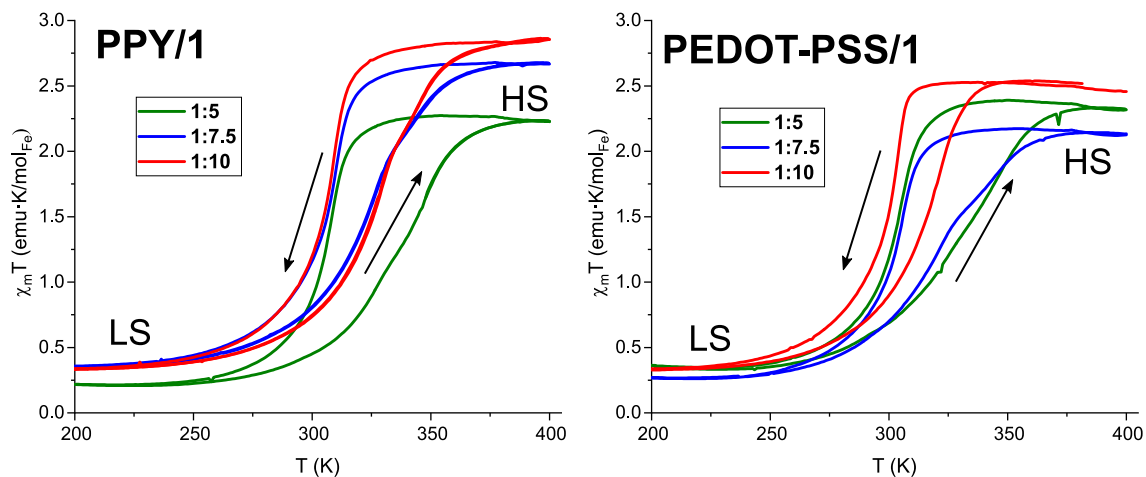
Figure S14. χ_mT versus T plots of all the organic polymer/**1** composites at a scan rate of 1 K/min in the 200−400 K range (ratio Polymer:SCO).

Table S4. Magnetic properties of all the composites (ratio Polymer:SCO).

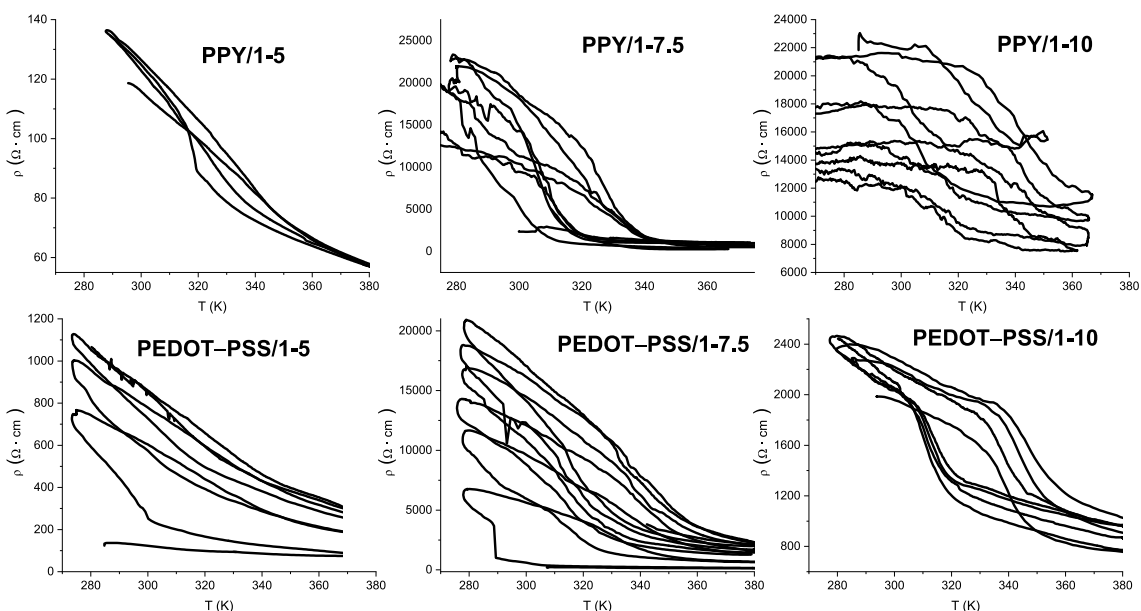| Sample	$T_{1/2}(\uparrow)$ [K]	$T_{1/2}(\downarrow)$ [K]	ΔT [K]	$\chi_mT(200\ \text{K})$ [emu·K/mol$_{Fe}$]	$\chi_mT(400\ \text{K})$ [emu·K/mol$_{Fe}$]
PPY/1-5	339	308	31	0.21	2.23
PPY/1-7.5	328	309	19	0.36	2.67
PPY/1-10	330	308	22	0.36	2.86
PEDOT/1-5	331	303	28	0.36	2.32
PEDOT/1-7.5	327	305	22	0.26	2.12
PEDOT/1-10	316	301	15	0.34	2.46

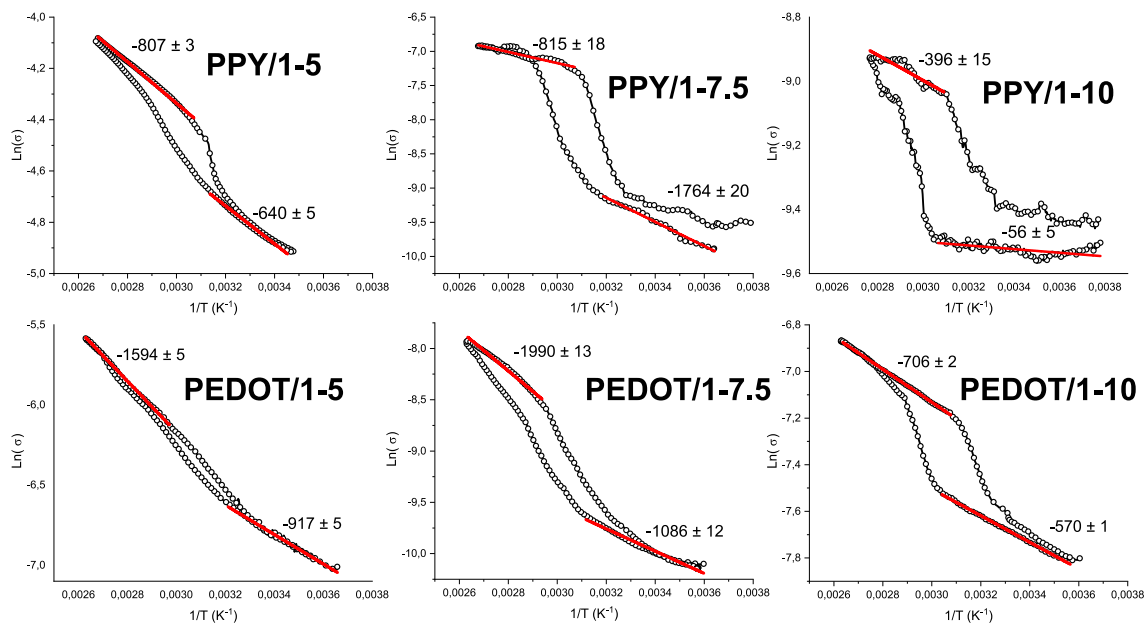**Figure S15**. Annealing process for organic polymer/**1** composites (Resistivity increases every cycle).

Figure S16. Ln (σ) vs 1/T and Arrhenius fittg for all the composites. (The numbers indicate the slope of the linear fittings).

Arrhenius Law:

$$Ln(\sigma) = Ln(\sigma_0) + \frac{-E_a}{k} \cdot \frac{1}{T}$$

Where σ_0 is the preexponential factor, k the Boltzmann constant (8.62 × 10^{-5} eV/K)and E_a the activation energy.

Table S5. E_a values in HS and LS obtained from the Arrhenius fitting.

Sample	E_a LS (eV)	E_a HS (eV)
PPY/1-5	0.055	0.069
PPY/1-7.5	0.152	0.070
PPY/1-10	0.005	0.034
PEDOT/1-5	0.079	0.137
PEDOT/1-7.5	0.094	0.171
PEDOT/1-10	0.049	0.061

References

1   H. M. Rietveld, Line profiles of neutron powder-diffraction peaks for structure refinement, *Acta Crystallogr.*, 1967, **22**, 151-152.